INNOVATIVE ENERGY ABSORBING MOUNTING SYSTEMS FOR HIGH MASS ROTORCRAFT PAYLOADS

William Kong, Chandrashekhar Tiwari, Matthew J. Hagon, Charles E. Bakis, Edward C. Smith
The Pennsylvania State University
University Park, PA, 16802

Michael A. Yukish
The Applied Research Laboratory
State College, PA, 16801

ABSTRACT

This paper presents recent developments on two innovative types of crashworthy cargo restraints for high mass rotorcraft payloads: textile-based devices and flexible matrix composite devices. Each type of device employs energy dissipation mechanisms to arrest the motion of payloads and limit the maximum load transmitted to tie-down points, thereby maintaining control over payload motion and improving crew survivability in the event of a crash or hard landing. The benefit of these devices over traditional devices is in their several-fold improvement in specific energy absorption capability, which leads to less parasitic mass and, therefore, facilitates the process of restraining cargo for cargo handling crews. Progress to-date includes the development of analytical models of both types of devices and experimental validation of the model for textile devices. A system model is also being developed to allow for the future specification of crashworthy restraint approaches for high mass payloads in rotorcraft.

1. INTRODUCTION

In the event of a crash or hard landing, high g-forces can cause cargo and other high mass items to break loose from their restraints and mounting points. The dangers of out-of-control cargo are severe and could even lead to fatalities in what could otherwise be considered a survivable situation. Thus it is in the interest of saving lives that new crashworthy cargo restraint concepts need to be developed to secure both the cargo and other high mass objects in a crash or hard landing. With increasing payload requirements for future heavy-lift rotorcraft, such as that under investigation in the Joint Heavy Lift program (Tenney, 2008); the forces required to arrest the motion of cargo in a crash will increase (FM 55-450-2, 1992). Cargo restraints will need to be improved to safely constrain movement of the cargo and limit the loads transmitted to the structure. Current restraint technologies used in military rotorcraft include steel chains, straps, nets and flexible barriers. In the event of a crash, the restraints or the mounting points (e.g. tie-down rings) can fail due to the lack of any load limiting capability in the restraint system. A load limiting restraint can dissipate the kinetic energy of the cargo as well as significantly reduce the forces transmitted to the mounting structure. This can lead to reductions in mass of the mounting structure, be it an automated cargo handling system or the actual airframe.

The current state-of-the-art in energy absorbing cargo restraints suffer from a low stroke-to-length ratio and low specific energy absorption (Desjardins et al., 1989; Hate et al., 1986). The stroke-to-length ratio is the ratio of the device's deployed to initial length. Specific energy absorption (SEA) is defined as the energy absorption per unit mass. The current state-of-the-art in load limiting technology is the wire bender concept which has an SEA of 3.6 J/g and a stoke-to-length ratio from 1 to 2. Cargo handling personnel have not embraced this technology because of uncertainties about required stroking distances and general dissatisfaction with the bulkiness and weight of available load limiting restraint systems. Therefore, the ease-of-use of any new cargo restraint device is an important design issue to address.

This paper presents the latest developments related to two innovative types of energy-dissipating, load-limiting cargo restraints: textile based devices and flexible matrix composite based devices. Functionally, both devices provide a designed load as a function of deployment distance, thus limiting attachment point loads while dissipating the kinetic energy of the payload during a crash. Work done to-date has focused on the development of analytical design tools for both types of devices. Experiments at various loading rates to validate the model have been conducted for the textile devices. A system model is currently being developed to provide a vehicle-level analysis to complement the device-level analyses.

2. TEXTILE-BASED DEVICES

Studies in the past have already demonstrated the advantages of textile-based stitch ripping devices (SRDs) for retaining high mass payload (Wess, 2004). Originally used by rock climbers and construction workers, the SRD is constructed by folding a strip of fabric and sewing the two halves together with thread as shown in Figure 1. When the applied load reaches the break strength of the

Report Documentation Page

Form Approved
OMB No. 0704-0188

1. REPORT DATE	2. REPORT TYPE	3. DATES COVERED
DEC 2008	**N/A**	**-**

4. TITLE AND SUBTITLE	5a. CONTRACT NUMBER
Innovative Energy Absorbing Mounting Systems For High Mass Rotorcraft Payloads	5b. GRANT NUMBER
	5c. PROGRAM ELEMENT NUMBER
6. AUTHOR(S)	5d. PROJECT NUMBER
	5e. TASK NUMBER
	5f. WORK UNIT NUMBER
7. PERFORMING ORGANIZATION NAME(S) AND ADDRESS(ES) **The Pennsylvania State University University Park, PA, 16802**	8. PERFORMING ORGANIZATION REPORT NUMBER
9. SPONSORING/MONITORING AGENCY NAME(S) AND ADDRESS(ES)	10. SPONSOR/MONITOR'S ACRONYM(S)
	11. SPONSOR/MONITOR'S REPORT NUMBER(S)

12. DISTRIBUTION/AVAILABILITY STATEMENT
Approved for public release, distribution unlimited

13. SUPPLEMENTARY NOTES
See also ADM002187. Proceedings of the Army Science Conference (26th) Held in Orlando, Florida on 1-4 December 2008, The original document contains color images.

14. ABSTRACT

15. SUBJECT TERMS

16. SECURITY CLASSIFICATION OF:			17. LIMITATION OF ABSTRACT	18. NUMBER OF PAGES	19a. NAME OF RESPONSIBLE PERSON
a. REPORT	b. ABSTRACT	c. THIS PAGE			
unclassified	**unclassified**	**unclassified**	**UU**	**8**	

Unladen Partially deployed

Figure 1. Photograph of a commercially available SRD.

stitches, a nearly constant load level is maintained as the fabric fold is ripped apart.

The specific energy absorption (SEA) for SRDs is 32 J/g, which is 9X better than wire benders. The importance of SEA as a design metric can be seen when considering future heavy lift rotorcraft which could have an 18,000 kg payload capability. The standard requirements for crashworthiness design include a 13 m/s impact velocity with 16 G peak acceleration (Desjardins et al., 1989). In this scenario, a wire bender mass of 422 kg is needed to arrest the cargo. In contrast, the required SRD mass is only 47 kg. The SRD is a strong candidate for crashworthy cargo restraint systems needing a high stroke-to-length ratio and high SEA. SRDs will be most effective for temporary cargo such as vehicles and various other palletized cargo thanks to its low weight and ease-of-use.

2.1 Analytical Model

The need for an analytical model stems from early efforts to improve SRD performance by varying webbing and thread materials and the number of stitches used (Wess, 2004). When comparing experimental data with an analysis using basic equations, a large gap existed between the theoretical and the actual results. There were some cases in which the theoretical values were more than double the experimental values. It was apparent that a better understanding of the underlying energy absorption mechanisms of the SRD was needed. Having a complete, fundamental model of the device is necessary to design a scaled up SRD for use as cargo restraints in future heavy-lift rotorcraft.

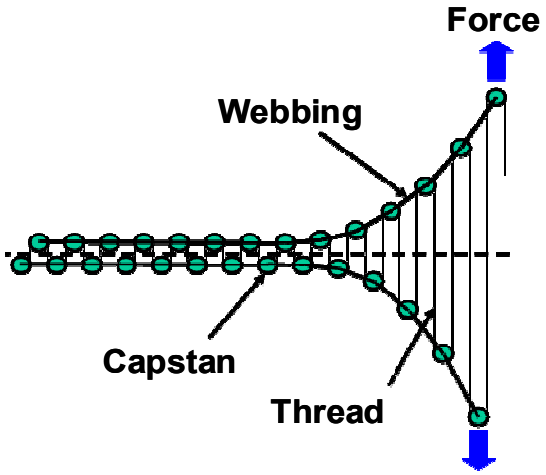

Figure 2. Simplified mechanical model of SRD.

In the analytical model currently in development (Hagon et al., 2007, 2008), the webbing is represented by a series of capstans connected by elastic links shown in Figure 2. A thread is sewn in-between the elastic links and around the capstans. Variables in the model include webbing modulus and cross-sectional area, thread modulus and cross-sectional area, thread strength, stitch pattern, and number of threads used to join the webbing. Using Equation (1), a thread tension distribution can be calculated for the entire SRD at each capstan.

$$\frac{T_{n+1}}{T_n} = e^{\mu\pi}, T_{n+1} > T_n \qquad (1)$$

The thread tension terms T_n and T_{n+1}, represent the tension in the threads on each side of a specific capstan. The coefficient of friction between the thread and the webbing, μ, is obtained experimentally. A system of equations relating the thread tensions, capstan displacement, stretch in the elastic links (webbing), and forces in the elastic links are solved simultaneously to obtain a thread tension distribution as shown in Figure 3.

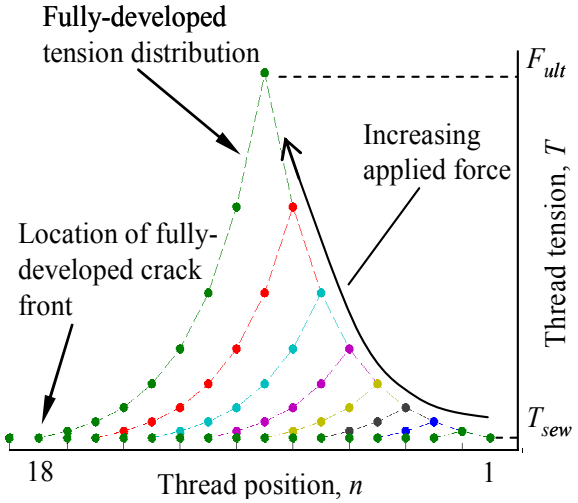

Figure 3. Thread distribution in SRD for different applied forces.

Each colored line in Figure 3 represents the thread tension distribution for a given applied force. The applied force on the SRD required to achieve a "fully-developed tension distribution" is the force required to drive the peak thread force to the failure strength of the thread, F_{ult}. The capstan position where F_{ult} occurs is the location of the first thread break. With the thread tension distribution

and SRD shape determined by the capstan analysis, a curve can be fit to the overall SRD displacement versus force relationship, which is valid only up to the point of thread rupture. Once a particular thread breaks, the capstan analysis is simply shifted along the length of the SRD and repeated up to the applied force needed to fail another thread. In this manner, the deployment of the SRD over multiple thread breaks can be simulated. Moreover, the energy dissipated by thread slip over the capstans and thread failure can be separately calculated and used to tailor the SRD design. Additional details of the capstan model are given by Hagon et al. (2008).

2.2 Quasi-static Tests

To validate the analytical model, quasi-static tests were conducted on a custom made SRD. The SRD was constructed of nylon webbing stitched together with a single polyester thread. A comparison between model predictions and experimental results can be seen in Figure 4. Until first thread rupture, the applied force required to break the first thread was predicted within 2% and the corresponding displacement within 9%. The location of the first thread rupture was predicted correctly as well.

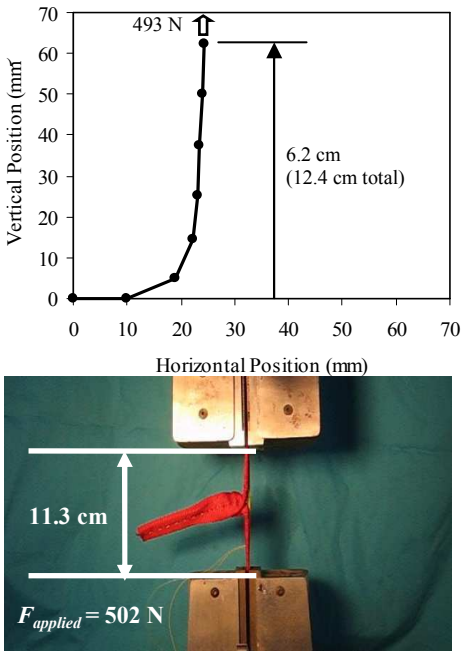

Figure 4. Comparison of profile shapes. Model predictions (above) and experiment (below) subsequent to the first thread rupture are shown.

Following the first thread rupture, load-displacement results from experimental tests did not correlate well with model predictions. Measured energies were 27-40% lower than the model predictions. There are several factors believed to be source of the overestimation in results, including nonlinear behavior of the material and the characteristics of SRD after first thread rupture. Future work calls for improvements to the model to take into account these factors.

2.3 Dynamic Tests

The SRD is designed to be used in a crashworthy cargo restraint system; therefore the device must be tested in dynamic loading conditions. Furthermore, SRDs are made of polymeric materials (e.g. nylon, polyester), which are known to behave differently under different loading rates. Dynamic testing of the SRD was conducted to compare quasi-static and dynamic behavior of commercial SRDs (Figure 5 and Figure 6, respectively). For the maximum initial velocity available on the test device (6 m/s), it is seen that there is more force fluctuation in the dynamic test than in the quasi-static test, although little change in the mean force is seen. According to the crashworthiness design guide developed by Simula Inc., the required design impact velocity is 13 m/s. Improvements to the test device are underway so that the SRD can be evaluated up to the required impact velocity.

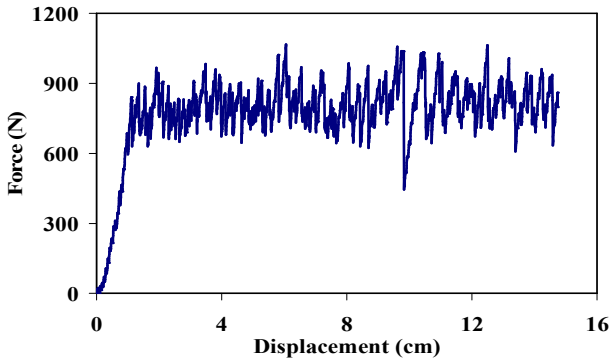

Figure 5. Sample results from quasi-static tests on commercial SRDs.

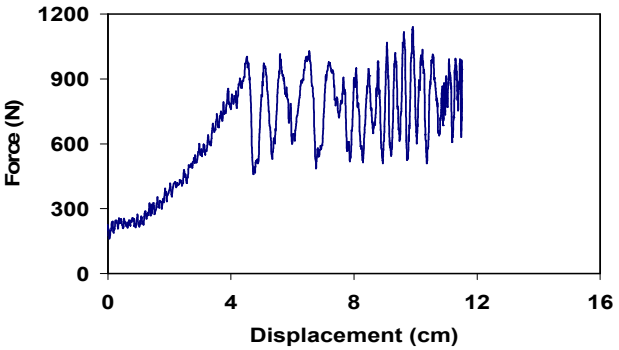

Figure 6. Sample results from dynamic tests on commercial SRDs, initial impact velocity of 6 m/s.

3. FMC TUBES

In addition to the textile based load limiters, an exploratory study on flexible matrix composite (FMC) tubes as novel energy absorbing devices was conducted. Two forms of composite tube load limiters were

investigated: crush tubes and tension-torsion SRD (TTSRD) tubes. Analytical models were developed for both concepts and an optimization study was conducted for the extension-twist tube concept.

3.1 Crush Tubes

Composite crush tubes feature angle-ply fiber reinforced elastomeric cylindrical tubes with a foam filling. The tubes are elastically tailored to have a Poisson's ratio of 6 to 8. When subject to an axial tensile load, the tubes deform non-linearly via fiber re-alignment to crush the foam filling. Energy is absorbed through plastic deformation of the foam filling.

3.2 Crush Tube Analytical Model

An analytical model was developed for the crush tube using carbon fiber FMC and several types of foam. Parameters required by the analysis are: tube geometry (e.g. radius, fiber angle, thickness), tube elastic properties, and foam material properties (crush stress, elastic properties). Each layer of the FMC tube has the properties shown in Table 1. The half-length of the tube is assumed to be 41.2 mm and the inner and outer radii are assumed to be 10.3 and 10.8 mm, respectively.

Table 1. Lamina properties of FMC tube.

Type	Long. Modulus (GPa)	Trans. Modulus (GPa)	Shear Modulus (GPa)	Poisson's Ratio
FMC	115	0.359	0.752	0.314

Angle-ply FMC tubes deform non-linearly under the applied axial load, primarily due to fiber realignment. A method to analyze non-linear axisymmetric deformation of an FMC tube with axial load and internal pressure was developed by Shan et al. (2006). In the FMC crush tube concept proposed here, an axial load stretches the tube and produces pressure on a foam core via the hoop-wise contraction of the tube. As a first cut approximation in the present analysis, the effect of the core on the FMC tube is assumed to be a constant internal pressure during the tensile load-up portion of a load cycle and no pressure during unloading. Using the model, various load vs. displacement curves can be plotted for different foam crush strengths, as shown in Figure 7 for a ±45-deg. FMC tube. Included in the figure is the unloading case, as well. The maximum force in Figure 7 is limited based on attainment of 2% strain in the fiber direction. The area enclosed by the load-up and unload curves is the energy absorbed by the device.

An increase in the crush stress of the foam translates to a proportional change in the load deflection curve and energy absorbed. Predicted SEA values of FMC crush tubes containing aluminum honeycomb filling

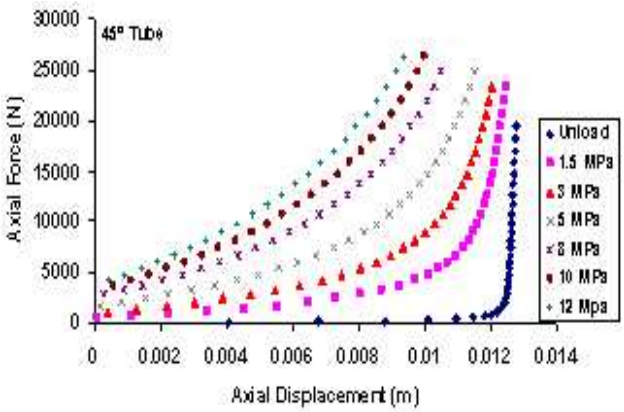

Figure 7. Load-Deflection curves for a ±45 deg FMC tube with varying crush stresses for the foam filling.

with variations in foam crush stresses and tube fiber angles are provided in Table 2.

The SEA values for crush tubes are highly influenced by the fiber orientation in the FMC tube, indicating a great potential for future device optimization. The fiber angles in which the peak SEA values are obtained also depend on the crush stress of the foam. The SEA values for crush tubes presented in Table 2 are greater than the wire bender SEA values. Additional variation of parameters revealed that a maximum SEA value of 21.5 J/g can be achieved with a ±45° FMC tube and an aramid/phenolic hexagonal honeycomb core with a crush stress of 10 MPa. As crush tubes are best suited for fixed cargo, a more fitting comparison would be with a basic metal tube which has an SEA of 10.2 – 13.5 J/g. To put things in perspective, the same example of restraining an 18,000 kg cargo can also be applied for crush tubes and metal tubes. For a metal tube with an SEA of 13.5 J/g, the mass of the device to arrest the cargo would be 113 kg; the mass of a crush tube with an SEA of 21.5 J/g would be 71 kg.

Table 2. Energy absorbed by crush tube for various fiber angles and crush stresses of aluminum honeycomb.

Crush Stress = 3.0 MPa					
Fiber Angle (deg)	25	35	45	55	65
SEA (J/g)	6.97	10.68	12.99	14.30	13.62
Crush Stress = 8.0 MPa					
Fiber Angle (deg)	25	35	45	55	65
SEA (J/g)	9.57	14.47	16.00	15.26	11.64

3.3 Extension-Twist Tubes

The extension-twist tube concept utilizes shear-extension elastic coupling in off-axis composite laminas.

The version of the extension-twist tube device presented here is a tension-torsion stitch ripping device (TTSRD). The device consists of two concentric extension-twist coupled cylindrical composite tubes with angles of fibers in opposite ($\pm\theta$) directions as shown in Figure 8. The inner tube is positioned inside of the outer tube and threads are used to stitch the two tubes together in a manner similar to that explained earlier for webbings in SRDs. A diagram of an assembled TTSRD is shown in Figure 9.

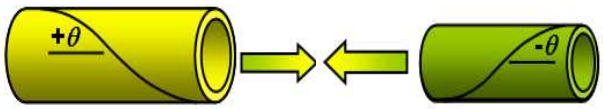

Figure 8. Extension twist coupled concentric tube.

When subjected to an axial tensile force, the inner and outer tubes have a tendency to twist in opposite directions. As the tubes twist, the tension in the thread increases until stitch rupture which leads to the dissipation of elastic energy. The envisioned application of TTSRDs is where low stroke and high stiffness are needed, such as in fixed payloads (overhead engine and transmission, various boxes containing electrical equipment, etc.). To explore the potential of TTSRD's in terms of the specific energy absorption (SEA), an analytical model was developed and used to carry out a parametric study.

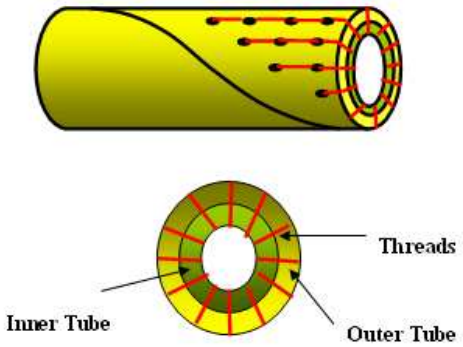

Figure 9. Sample stitch pattern of the TTSRD device.

3.4 Extension-Twist Tube Analytical Model

The mechanical model of the TTSRD takes into account several material and geometric parameters, including the composite material system, fiber angle, tube length and thickness, number of stitches and number of threads per stitch. Due to the absence of internal pressure loading, the tubes have zero hoop stress. The following assumptions have been made in the analysis:

1. For any stitched part of the tube, the total twist of the tube is assumed to be "zero". However, there exists an infinitesimal twist which loads the threads in tension and produces the Z-shape shown in Figure 10. At the laminate level, this assumption makes the shear strain equal to zero.

2. For any unstitched part of the tube, the shear force resultant is assumed to be zero.

3. If F is the total axial force acting on the device then the axial force on the inner tube is $F/2$.

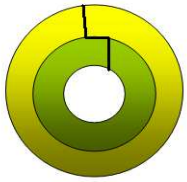

Figure 10. Cross section of TTSRD device showing infinitesimal twist.

The external force, F, at which threads break depends upon the thread and tube properties. On either tube, the shear force resultant required to break a circumferential row of threads, N_{xsb}, is given in Equation (2). The axial force resultant, N_{xxb}, is proportional to the shear force resultant as shown in Equation (3). The limit load of the device, F, is given by Equation (4).

$$N_{xsb} = 2 n_t n_c \sigma_{ult} (\pi d^2 / 4) / (2 \pi R) \quad (2)$$

$$N_{xxb} = K_{11} N_{xsb} / K_{12} \quad (3)$$

$$F = 4 \pi R N_{xxb} \quad (4)$$

In these equations, n_t is the number of threads in a stitch, n_c is the number of stitches in a cross section of the tube, σ_{ult} is the break strength of the thread material, d is the diameter of the thread, R is the radius of the tube, and K_{11} and K_{12} are the axial tube stiffness and extension-twist coupling, respectively. The K_{11} and K_{12} terms come from the stiffness matrix obtained after applying the assumptions previously mentioned.

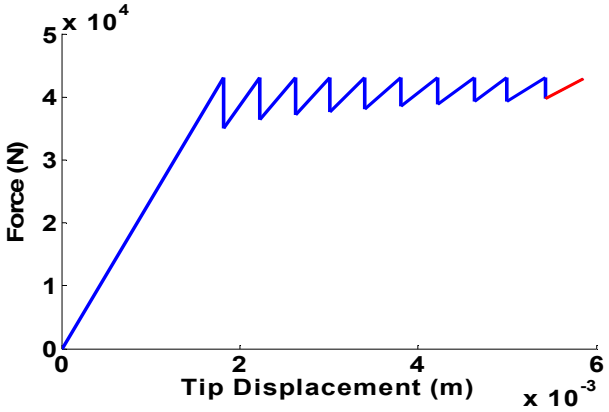

Figure 11. Force vs displacement curve for an FMC TTSRD.

A sample force vs. displacement curve from a model simulation is shown in Figure 11. The simulation was for a TTSRD device made of FMC materials. The value at which the force-displacement curve peaks is the limit load for the device. Every peak in the curve corresponds to rupture of a circumferential row of stitches. When all the stitches fail, the tubes are decoupled and are loaded individually until ply failure occurs. This region is marked by the "red" slope after the first 10 peaks (the device had 10 stitches along the length). The total area under the force vs. displacement curve is the amount of energy dissipated by the device. The total axial displacement of the location of the applied force (i.e. tip displacement) until all the stitches break is defined as the stroke of the device. It can be seen that the force vs. displacement curves for the TTSRD are similar to those of textile-based SRDs. The response, however, is considerably stiffer.

The amount of energy absorbed by the device varies significantly with the selection of parameters. An example of the effect of varying fiber angle is shown in Figure 12. The SEA for carbon FMC TTSRD tubes range from 1.8 J/g to 8.1 J/g. To restrain an 18,000 kg payload, a TTSRD device would have a mass of 187 kg, which is heavier than metal tubes, but lighter than wire benders. However, there is a possibility for better SEA values if the TTSRD tube is filled with a foam core, thus combining the features of TTSRDs and crush tubes.

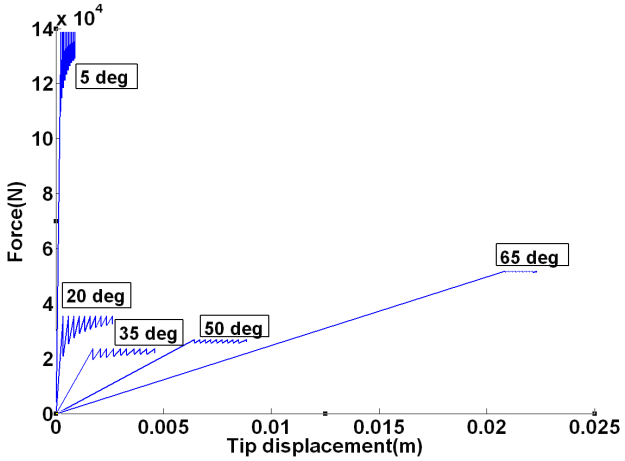

Figure 12. Model results for FMC TTSRDs with variation in fiber angle.

A simulated annealing based optimization routine for TTSRD tubes was developed. The optimization constraints of ply failure were based upon the failure envelopes given by Maximum stress or Tsai- Wu criteria (Herakovich et al.,1998; Daniel et al., 2006). These envelopes displayed a large variation with respect to different composite systems selected. On the basis of the mentioned failure envelopes, a parametric optimization was conducted to maximize the SEA of the device. Table 3 shows the results of the optimization study for different tube material systems.

Table 3. Optimized TTSRD tube SEA values (J/g) for various tube material systems.

	Carbon FMC	Carbon/ Epoxy	E-Glass/ Epoxy	Kevlar/ Epoxy
Max Stress	1.8	2.05	7.1	2
Tsai-Wu	8.1	2.01	4.5	3.2

The optimized force vs. displacement curve for TTSRDs using carbon FMC tubes is shown in Figure 13. It can be seen that different limit loads can be obtained through the material selection and the objective function chosen to be maximized. If the objective function to be optimized was the peak load or the stroke of the device, a different set of optimal parameters would be produced. In this study, the constraints included in the analysis are based only upon the ply failure criterion of the composite materials; other constraints can easily be included in the analysis depending upon the requirements of the end user.

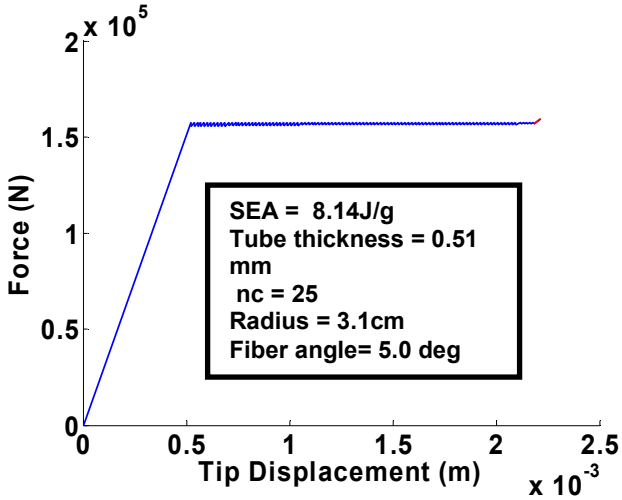

Figure 13. Optimized force-deflection curve.

4. SYSTEM MODEL

A vehicle-level analysis is needed to understand how the SRDs will be used as part of a cargo restraint system. Thus, a system model is currently being developed for a comprehensive vehicle analysis.

The development of the system model can be split up into two phases. The first phase, which is currently underway, focuses on the dynamics of restrained cargo in a crash. The number and type of restraints used, including limit force and stroke/length ratio, are determined by the particular vehicle under consideration. It is essential to prevent the cargo from colliding with the cabin walls and

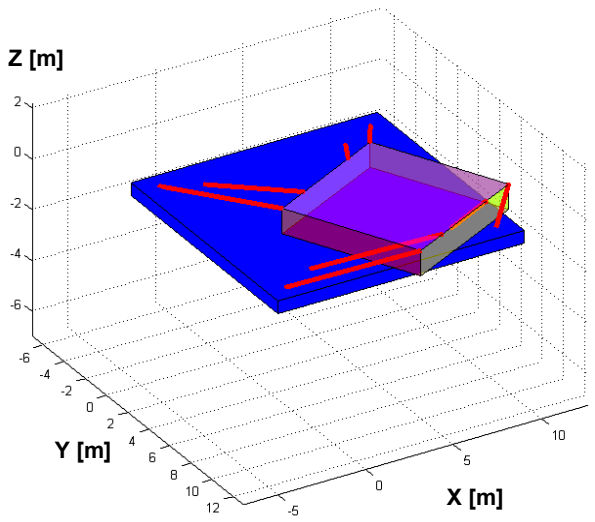

Figure 14. Screenshot from system model video animations showing the cargo (multi-colored box) tied down by cargo restraints (red lines) inside the aircraft (blue platform).

to keep a safe distance from any passengers and crew. In the second phase, which has not been started yet, the aim will be to assess by structural analysis the loads introduced to the airframe during a high-g event, and to determine the vehicle-level weight savings that can be gained by using load-limiting payload mounting devices as opposed to rigid devices such as chains.

4.1 Dynamic Analysis

The movement of cargo in the event of a crash is a key aspect of the system model. The model analyzes a 6-DOF system with two rigid bodies: a box and a platform representing the cargo and aircraft, respectively. The model can analyze the dynamics of a crash at any orientation or impact velocity. Additionally, the model is able to analyze any type of cargo restrained by any number of restraints in various configurations. The cargo is visually fixed as a box, but the location of the cargo CG and restraint attachment points on the cargo are variable parameters. In addition to restraint attachment points and cargo/platform geometry, other variable model parameters include cargo/platform mass, maximum device stroke, activation force for load limiter and initial conditions for displacement, velocity, rotation, and angular velocity. The system model output includes video animations which are used to visualize the dynamics of cargo movement, as shown in Figure 14.

Unlike rigid restraints (e.g. chains), energy absorbing cargo restraints will stroke and allow the cargo to move. The system model can analyze cargo movement based on a given number of restraints and tie-down configuration. The configuration of the restraints is

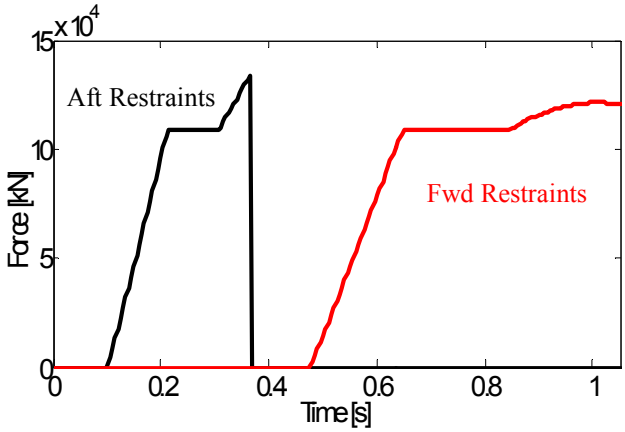

Figure 15. Plot of restraint forces from model simulation.

dependent on the location of tie-down rings on the cabin floor as well as the strength of the tie-down rings.

4.2 Structural Analysis

Future work will focus on experimentally validating the dynamics of the model (i.e. first phase) as well as the second phase of the model: structural analysis. This aspect of the system model is also required to determine the number of restraints used as well as the new strength requirements of the airframe.

An example of the restraint forces from a model simulation is shown in Figure 15. The simulation parameters match the crash requirements of a 13 m/s forward longitudinal impact velocity. The 18,000 kg cargo is tied down by four restraints: one restraint per corner. Since the cargo is a symmetric box and the impact is purely longitudinal, the force vs. time response of the two restraints located aft of the cargo box are identical; the forces of the two restraints located at the forward end of the cargo box are also identical. The aft restraints are first to activate and are represented by the black line. The restraints on the forward end of the cargo will be engaged last as shown by the red line. The simulation shows that the two aft restraints are not sufficient to arrest the cargo and fail. The cargo continues to move until the forward restraints are engaged to finally arrest the cargo.

The restraints were modeled as an idealized textile-based load limiter which can undergo an initial elastic load-up, a constant-force stroke, and a final elastic load-up once the designed stroke range has been exceeded. The activation force of the restraints for this particular simulation was 200 kN. It is possible to use the characteristics of a specific type of load limiter (e.g. SRD, FMC tubes).

CONCLUSIONS

Textile based load limiters, which are ideal energy dissipating tie-downs for temporary cargo and situations without low stroke and high stiffness requirements, promise a much improved specific energy absorption capability (9X) over wire-bender technology and can be easily integrated with current cargo tie-down systems and procedures. An analytical model of the SRD was developed that accounts for webbing stretch, thread slippage and thread rupture in the energy absorption calculations. Quasi-static testing of the SRD has shown that the model can correctly predict SRD performance up until the first thread rupture. However, further work is needed to improve the SRD model predictions after first thread rupture; validate the model for up-scaled SRDs; and to design stitch patterns for improved greater energy dissipation without added mass.

Dynamic testing of SRDs has shown negligible rate effects on energy absorption for impact velocities up to 6 m/s. Future testing will be aimed at achieving the desired impact velocity of 13 m/s to satisfy crashworthiness design requirements.

FMC tube concepts, which are best suited for cargo restraints with low stroke constraints, show the potential for greater specific energy absorption capability over conventional materials such as metals. For the specified material systems considered in the present study, the crush tube concept had a maximum SEA of 21.5 J/g with a ±45° FMC tube and an aramid/phenolic hexagonal honeycomb core with a crush stress of 10 MPa. The TTSRD concept exhibited optimized SEA values ranging from 1.8 J/g to 8.1 J/g, depending upon the failure criterion and the material used. Future work for FMC tubes will include improvements to the analytical models, continuing optimization studies, building and testing of FMC tubes, and integration of the TTSRD and crush tube concepts into a single device.

Comparisons with wire benders have shown that textile based and FMC tube devices have a distinct advantage over what is currently considered the state-of-the-art in load limiters in terms of specific energy absorption. For the example of restraining an 18,000 kg cargo in a crash with an impact velocity of 13 m/s, SRD devices had the lowest mass (47 kg) followed by crush tubes (71 kg) and TTSRDs (187 kg). The SRD and crush tube devices are both lighter than the wire bender (422 kg) and metal tube (113 kg). The TTSRD, however, exhibits lower SEA values than metal tubes. It is expected that combining features of the TTSRD and crush tube will result in an SEA value exceeding that of a metal tube.

The first phase of the system model is underway. The model is able to create video animations to analyze the dynamics of restrained cargo during a crash event. Future work for the system model will focus on structural analysis and experimental validation of the model.

ACKNOWLEDGEMENTS

This research was partially funded by the Office of Naval Research under the Award No. N00014-08-C-0420. The U.S. Government is authorized to reproduce and distribute reprints notwithstanding any copyright notation thereon. Any opinions, findings and conclusions or recommendations expressed in this publication are those of the authors and do not necessarily reflect the views of the Office of Naval Research. The authors also thank Prof. Ashok Belegundu of Penn State for his help in parametric optimization routines.

REFERENCES

Daniel, I. M., and Ishai, O., 2006: Engineering Mechanics of Composite Materials, 2nd Edition, Oxford University Press.

Desjardins, S. P., Zimmermann, R. E., Bolukbasi, A. O. and Merritt, N. A., 1989: Aircraft Crash Survival Design Guide, vol. 4, USAAVSCOM TR-89-D-22D.

FM 55-450-2, 1992: Army Helicopter Internal Load Operations. *Department of the Army*.

Hagon, M. J., Bakis, C. E., Yukish, M. A., and Smith, E. C., 2007: A New Look at Lightweight Energy Absorbing Devices for Heavy Cargo Restraints, *American Helicopter Society 63rd Annual Forum*, Virginia Beach, VA.

Hagon, M. J., Bakis, C. E., Yukish, M. A., and Smith, E. C., 2008: Energy-Absorbing Textile Devices for Heavy Cargo Restraints, *American Helicopter Society 64th Annual Forum*, Montréal, Canada.

Hate, R. L., Campbell, R. F., George, H. L., and Shefrin, J., 1986: State-of-the-Art Crashworthy Mounting Systems for Military Aircraft, *National Specialist's Meeting on Crashworthy Design of Rotorcraft*, Atlanta, GA.

Herakovich, C. T., 1998: Mechanics of Fibrous Composites, John Wiley & Sons, Inc., NY.

Shan, Y., Philen, M. P., Bakis, C. E., Wang, K. W., Rahn C. D., 2006: Nonlinear-elastic Finite Axisymmetric Deformation of Flexible Matrix Composite Membranes Under Internal Pressure and Axial Force, *Composite Science and Technology,* **66**, 3053-3063.

Tenney, B. S., 2008: Joint Heavy Lift Full Steam Ahead, *Vertiflite,* **54** , 18-20.

Wess, D.B., 2004: Aircraft Restraint Mechanism, Technical Memorandum 04-094, Applied Research Laboratory, State College, PA.